Off-resonance coupling between a cavity mode and an ensemble of driven spins

Hui Wang, Sergei Masis, Roei Levi, Oleg Shtempluk, and Eyal Buks
Andrew and Erna Viterbi Department of Electrical Engineering, Technion, Haifa 32000, Israel
(Received 6 January 2017; revised manuscript received 1 March 2017; published 22 May 2017)

We study the interaction between a superconducting cavity and a spin ensemble. The response of a cavity mode is monitored while simultaneously the spins are driven at a frequency close to their Larmor frequency, which is tuned to a value much higher than the cavity resonance. We experimentally find that the effective damping rate of the cavity mode is shifted by the driven spins. The measured shift in the damping rate is attributed to the retarded response of the cavity mode to the driven spins. The experimental results are compared with theoretical predictions and fair agreement is found.

DOI: 10.1103/PhysRevA.95.053853

I. INTRODUCTION

Cavity quantum electrodynamics (CQED) [1] is the study of the interaction between matter and photons confined in a cavity. In the Jaynes-Cummings model [2], the matter is described using the two-level approximation and only a single-cavity mode is taken into account. The interaction has a relatively large effect on the cavity mode response when the ratio $E/\hbar\omega_{\mathrm{a}}$ between the energy gap E separating the two levels and the cavity mode photon energy $\hbar\omega_{\mathrm{a}}$ is tuned close to unity. Recently, it was experimentally found that the cavity response exhibits higher-order resonances in the nonlinear regime when the ratio $E/\hbar\omega_{\mathrm{a}}$ is tuned close to an integer value larger than unity [3].

In the current study, we explore the case where $E/\hbar\omega_{\mathrm{a}} \gg 1$ [4]. This is done by investigating the interaction between an ensemble of spins and a superconducting cavity mode [5–7]. The energy separation between the spin energy eigenstates, which is given by $E = \hbar\omega_{\mathrm{L}}$, where ω_{L} is the Larmor frequency, is tuned to a value much higher than the cavity mode photon energy $\hbar\omega_{\mathrm{a}}$. For this case, the CQED interaction is expected to be negligibly small in the regime of weak driving. On the other hand, with an intense driving at an angular frequency close to ω_{L}, we observe a significant change in the cavity mode response.

In the current experiment, the cavity mode effective damping rate is measured as a function of the spin driving amplitude and detuning frequency. The observed shift in the effective damping rate is attributed to the retarded response of the cavity mode to the driven spins. Related effects of Sisyphus cooling, amplification, lasing, and self-excited oscillation have been theoretically predicted in other systems having a similar retarded response [8–12].

II. EXPERIMENT

Significant change in the response of the measured cavity mode of angular frequency ω_{a} is possible only when intense driving is applied to the spins. In order to allow sufficiently strong driving, the spin ensemble is coupled to an additional cavity mode having angular frequency $\omega_{\mathrm{b}} \gg \omega_{\mathrm{a}}$. When the Larmor frequency ω_{L} is tuned to a value close to ω_{b}, the additional cavity mode allows enhancing the spin driving amplitude.

A sketch of the device is seen in Fig. 1. It is made of two sapphire wafers and a high-resistivity silicon wafer that are attached together to form a dual band resonator. A radio-frequency resonator of angular frequency ω_{a} is constructed by integrating an inductor in the shape of the Greek letter Ω [13] made on the bottom sapphire wafer, and two capacitors in series, which are formed between the two sapphire wafers. A square hole is made in the upper sapphire wafer in order to allow insertion of the silicon wafer, which carries a spiral-shaped microwave resonator having angular frequency ω_{b} [14,15].

Both of the resonators are designed to be efficiently coupled to the spin ensemble of diphenylpicrylhydrazyl (DPPH) powder, placed between them. This radical, which contains three benzene rings, has a single unpaired electron, which gives rise to a Landé g-factor of 2.0036 [16,17]. A sketch of the experimental setup is seen in Fig. 2. A loop antenna is employed for delivering input and output signals to both resonators.

The measured reflectivity near the electron spin resonance (ESR) of the omega and spiral resonators is seen in Figs. 3(a) and 3(b), respectively [18]. Fitting the data with theory (e.g., Eq. (4) of Ref. [3]) allows extracting the value of the coupling coefficient g_{a} (g_{b}), which characterizes the interaction between the spin ensemble and the omega (spiral) resonator, and which is found to be $g_{\mathrm{a}} = 13$ MHz ($g_{\mathrm{b}} = 83$ MHz).

The linear response of the decoupled omega resonator is characterized by a complex angular frequency given by $\omega_{\mathrm{a}} - i\gamma_{\mathrm{a}}$, where γ_{a} is the mode damping rate. The effect of coupling on the linear response of the mode can be described in terms of an effective complex angular frequency $\Omega_{\mathrm{a}} = \omega_{\mathrm{a}} - i\gamma_{\mathrm{a}} + \Upsilon_{\mathrm{a}}$, where Υ_{a} represents the coupling-induced frequency shift. The complex angular frequency Ω_{a} can be extracted from the line shape of the measured cavity reflectivity vs frequency curves. The change in the damping rate, $-\operatorname{Im}\Upsilon_{\mathrm{a}}$, is seen in the color-coded plots of Fig. 4 as a function of the Larmor frequency ω_{L} and the spin driving angular frequency ω_{p}.

III. THEORY

To account for the experimental findings, two possible contributions to Υ_{a}, which is expressed as $\Upsilon_{\mathrm{a}} = \Upsilon_{\mathrm{aL}} + \Upsilon_{\mathrm{ab}}$, have been theoretically estimated. While Υ_{aL} represents the shift induced by the coupling to the driven spins, the Υ_{ab} contribution originates from the coupling to the driven spiral mode.

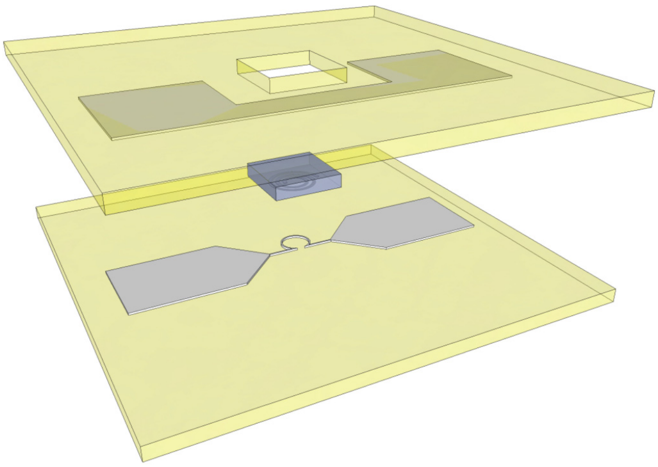

FIG. 1. The device is made of two 40×40×0.5 mm sapphire wafers carrying the radio-frequency omega resonator, and a 5×5×0.5 mm silicon wafer carrying the microwave spiral resonator. The DPPH powder is placed between the omega inductor and the spiral. The three wafers are vertically shifted in the sketch for clarity. In the assembled device, both the top sapphire wafer and the silicon wafer are placed directly on top of the bottom sapphire wafer. The three wafers and a loop antenna are assembled together inside a package made of high-conductivity oxygen-free copper. Both omega and spiral resonators are made by dc-magnetron sputtering of a 200-nm-thick niobium layer. The radius of the omega inductor is 500 μm and the linewidth is 40 μm. The spiral dimensions are inner radius 500 μm, outer radius 580 μm, linewidth 10 μm, and number of turns 4. The measured frequency of the omega (spiral) resonator is $\omega_a/2\pi = 0.173$ GHz ($\omega_b/2\pi = 2.00$ GHz), whereas the value obtained from numerically simulating the structure is 0.176 GHz (2.07 GHz).

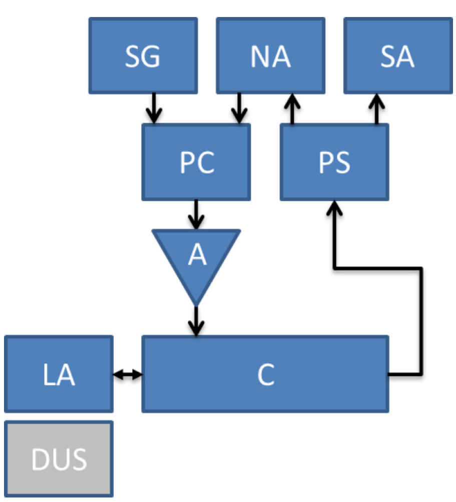

FIG. 2. The experimental setup. A power combiner (PC) is employed for combining the injected signals of a signal generator (SG) and a network analyzer (NA). The combined injected signal is transmitted through an amplifier (A) and a coupler (C), and feeds the loop antenna (LA), which is positioned above the device under study (DUS). The back-reflected signal is split by a power splitter (PS) and measured by both a NA and a spectrum analyzer (SA).

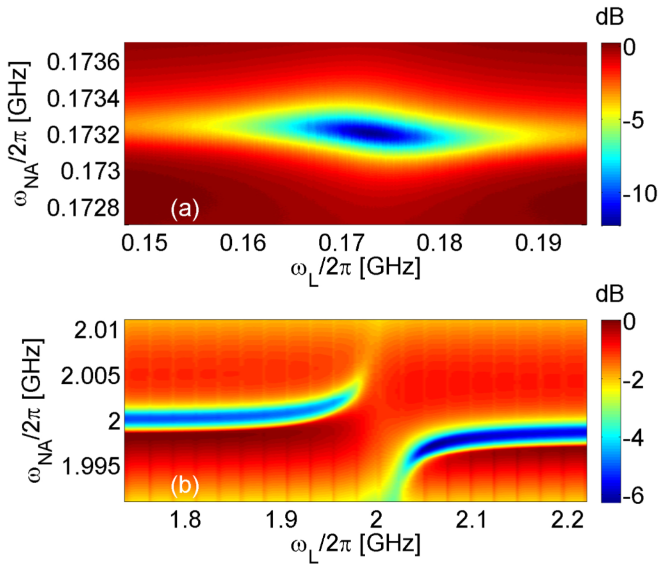

FIG. 3. ESR of (a) the omega and (b) the spiral resonators. The color-coded plots display the measured reflectivity coefficient $|S_{11}|^2$ vs ω_L (i.e., vs static magnetic field) and the probing frequency ω_{NA}. Measurements are performed by a network analyzer at a temperature of $T = 3.1$ K, for which the polarization coefficient p_0 [see Eq. (A20)] is given by $p_0 = -1.4\times10^{-3}$ ($p_0 = -1.6\times10^{-2}$) for the omega (spiral) resonator.

A magnetic field having two mutually orthogonal components, i.e., a static component and an alternating one at an angular frequency ω_p, is applied to the spin ensemble. The amplitude of the static (alternating) component is $\gamma_g^{-1}\omega_L$ ($\gamma_g^{-1}\omega_1$), where γ_g is the electron spin gyromagnetic ratio. The frequency shift Υ_{aL} is found to be given by [see Appendix A and Eq. (A46)]

$$\Upsilon_{aL} = \frac{\dfrac{\frac{8g_a^2\omega_1^2}{\omega_a^2\gamma_2}\frac{\Delta_{pL}}{\gamma_2}\left(i-\frac{2\gamma_2}{\omega_a}\right)}{1+\frac{\Delta_{pL}^2}{\gamma_2^2}+\frac{4\omega_1^2}{\gamma_1\gamma_2}}p_0}{\frac{\gamma_1}{\omega_a}\left(\frac{\omega_R^2+\eta\omega_a^2}{\omega_a^2}-1\right)-i\left(\frac{\omega_R^2}{\omega_a^2}-1\right)}, \tag{1}$$

where $\Delta_{pL} = \omega_p - \omega_L$ is the detuning, γ_1 (γ_2) is the longitudinal (transverse) spin relaxation rate, p_0 is the spin polarization in thermal equilibrium [see Eq. (A20)], $\omega_R = \sqrt{4\omega_1^2 + \Delta_{pL}^2}$ is the Rabi frequency of the driven spins, and η is given by $\eta = (2\gamma_2/\gamma_1)[2\omega_1^2(1-\gamma_1/\gamma_2)/\omega_a^2 - 1]$ [see Eq. (A47)]. Note that Eq. (1) is obtained by assuming that $|\Delta_{pL}| \ll \omega_L$, $\gamma_a \ll \omega_a$ and $\gamma_1,\gamma_2 \ll \omega_a$.

The real part of Υ_{aL} is the cavity mode angular frequency change that is induced by the coupling to the driven spins, whereas the imaginary part is $-\gamma_{aL}$, where γ_{aL} denotes the change in cavity mode damping rate. The dependence of the normalized change in damping rate γ_{aL}/ω_a on the normalized detuning Δ_{pL}/ω_a and the normalized driving amplitude ω_1/ω_a is shown in Fig. 5(a). When the driving is red detuned, i.e., when Δ_{pL} is negative, the change in damping rate γ_{aL} is positive and, consequently, mode cooling is expected to occur [19]. The opposite behavior occurs with blue detuning, i.e., when Δ_{pL} is positive.

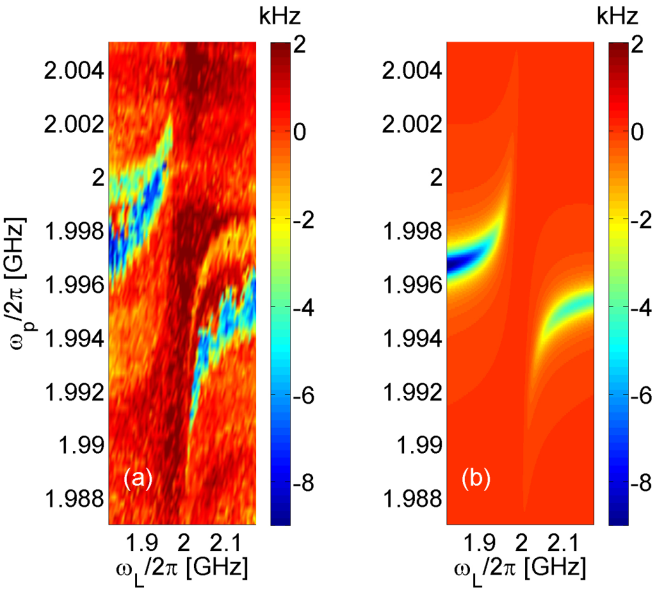

FIG. 4. The (a) measured and (b) calculated change in the damping rate $-\mathrm{Im}\,\Upsilon_a$ vs ω_L and the pump frequency ω_p. The experimental value is obtained from the line shape of the omega resonance. The Larmor frequency ω_L is tuned by applying a static magnetic field in a direction parallel to the wafers. The pump power is set to the value 17 dBm, which corresponds to a driving amplitude of $\omega_1/2\pi = 12$ MHz. (b) The calculated shift is based on Eqs. (1) and (2). The following parameters are used in the calculation: $\gamma_b = 0.4$ MHz and $\gamma_2 = 8.3$ MHz (other parameters are specified above).

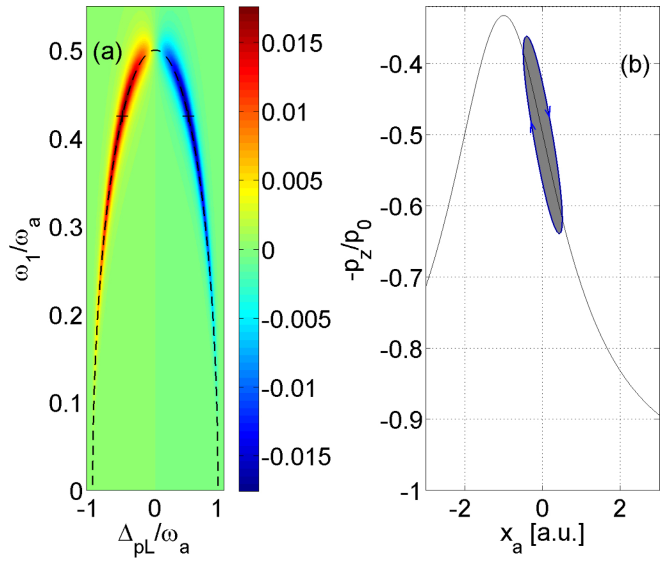

FIG. 5. The contribution to cavity mode damping rate γ_{aL} due to coupling to the driven spins. (a) The normalized contribution γ_{aL}/ω_a vs normalized detuning Δ_{pL}/ω_a and normalized driving amplitude ω_1/ω_a. The calculation is based on Eq. (1) with the following assumed parameters: $\gamma_1/\omega_a = 2\gamma_2/\omega_a = 0.05$, $g_a/\omega_a = 0.1$, and $p_0 = -0.1$. (b) Normalized spin polarization $-p_z/p_0$ vs cavity mode amplitude x_a for the case of blue-detuned driving. The black solid line represents the steady-state normalized spin polarization $-p_{z0}/p_0$. Retardation in the response of the spins to periodic oscillation of x_a is illustrated by the blue closed curve.

For both cases, large change in the effective cavity mode damping rate occurs near the overlaid dotted line in Fig. 5(a), along which the Rabi frequency ω_R coincides with the cavity mode frequency ω_a, i.e., $\Delta_{pL} = \pm\sqrt{\omega_a^2 - 4\omega_1^2}$. This behavior can be explained by noticing that along the dotted line, i.e., when $\omega_R = \omega_a$, the imaginary part of the denominator of Eq. (1) vanishes and, consequently, $|\Upsilon_{aL}|$ reaches a maximum. The largest change in the damping rate, which is denoted by $\gamma_{aL,\,max}$, can be evaluated by analyzing the expression given by Eq. (1). In the absence of spin dephasing, i.e., when $\gamma_1/\gamma_2 = 2$, it is found that the largest change, which is given by $\gamma_{aL,\,max} \simeq 0.437 \times g_a^2 p_0/\gamma_2$, occurs at the points $(\Delta_{pL}/\omega_a, \omega_1/\omega_a) \simeq (\pm 0.527, 0.425)$, which are labeled by crosses in Fig. 5(a). In the current experiment, however, these points are not accessible since $\omega_1 \ll \omega_a$.

The underlying mechanism responsible for the change in the effective cavity mode damping rate is similar to a related mechanism occurring in optomechanical cavities [19]. The coupling to the spins gives rise to a forcing term acting on the cavity mode, which is proportional to the spin polarization p_z [see Eq. (A11)]. On the other hand, the same coupling effectively shifts the Larmor frequency of the spins [see Eq. (A12)] and, consequently, the effective spin driving detuning $\Delta_{pL,eff} = \Delta_{pL} + g_a x_a$ becomes dependent on the cavity mode amplitude x_a [see Eq. (A25)].

For any fixed value of the cavity mode amplitude x_a, the spin polarization p_z in the steady state, which is denoted by p_{z0}, can be calculated using Eq. (A43) below. The dependence of p_{z0} on x_a is demonstrated by the solid black line in Fig. 5(b) for the case of blue-detuned spin driving. Consider first the adiabatic limit, for which it is assumed that $\omega_a \ll \gamma_{1,2}$. For this case, the dynamics of the cavity mode is assumed to be relatively slow and, consequently, the spin polarization p_z is expected to remain very close to the steady-state value given by p_{z0}, i.e., to adiabatically follow the x_a-dependent instantaneous steady-state value. Therefore, no change in the cavity mode damping rate is expected in the adiabatic limit.

Large deviation between the momentary polarization p_z and the steady-state value p_{z0} is possible in the nonadiabatic case, for which the response of the spins to the time evolution of the cavity mode becomes retarded. The closed curve in Fig. 5(b) represents the periodic time evolution of p_z for the case where the cavity mode oscillates at a fixed amplitude at its resonance frequency around the point $x_a = 0$. Since p_z is proportional to the force acting on the cavity mode, the area colored in gray in Fig. 5(b) is proportional to the net work done on the cavity mode per cycle. While the area is positive for the case of blue detuning, which is the case demonstrated by Fig. 5(b), red detuning gives rise to negative values, i.e., to energy flowing away from the cavity mode. These affects of energy flow between the cavity mode and the driven spins give rise to the above-discussed change in the effective cavity mode damping rate.

The frequency shift due to the driven spiral mode is attributed to an intermode coupling term in the Hamiltonian of the coupled system, which is assumed to be given by $K(A_a + A_a^\dagger)(A_b + A_b^\dagger)^2$, where A_a (A_b) is an annihilation operator of the omega (spiral) resonator, and K is the intermode coupling coefficient [see Eq. (B1)]. The contribution Υ_{ab} is found to be given by [see Appendix B and Eqs. (B19) and (B30)]

$$\Upsilon_{\mathrm{ab}} = \frac{4K^2|F_{\mathrm{bf}}|^2}{\omega_{\mathrm{D}}^2+\gamma_{\mathrm{b}}^2} \times \left\{ \frac{\frac{\omega_{\mathrm{D}}}{\gamma_{\mathrm{b}}^2}}{\left[\frac{i(\omega_{\mathrm{a}}-\omega_{\mathrm{D}})}{\gamma_{\mathrm{b}}}-1\right]\left[\frac{i(\omega_{\mathrm{a}}+\omega_{\mathrm{D}})}{\gamma_{\mathrm{b}}}-1\right]} + \frac{1+\frac{i\gamma_{\mathrm{b}}}{\omega_{\mathrm{s}}}}{\omega_{\mathrm{s}}} \right\}, \tag{2}$$

where F_{bf} and ω_{D} are the amplitude and angular frequency detuning, respectively, of the spiral mode driving, ω_{b} and γ_{b} are the spiral mode angular frequency and damping rate, respectively, and $\omega_{\mathrm{s}} = 2\omega_{\mathrm{b}} - \omega_{\mathrm{a}}$. Note that when $\gamma_{\mathrm{b}} \ll \omega_{\mathrm{a}}$ and $\gamma_{\mathrm{b}} \ll \omega_{\mathrm{s}}$, the first term in the second row of Eq. (2) becomes negligibly small provided that $|\omega_{\mathrm{D}}| \ll \omega_{\mathrm{a}}^2/\omega_{\mathrm{s}}$.

IV. DISCUSSION

As can be seen from the comparison between Figs. 4(a) and 4(b), fair agreement is obtained between data and theory. Reasonable agreement cannot be obtained unless both contributions Υ_{aL} [Eq. (1)] and Υ_{ab} [Eq. (2)] are taken into account. The contribution of Υ_{ab} is dominated by the second term in the second row of Eq. (2).

Our results demonstrate the ability to modify the effective damping rate of a cavity mode by driving spins that are coupled to the mode. Red-detuned driving provides a positive contribution to the damping rate, whereas negative contribution can be obtained by blue-detuned driving. For the former case, this effect can be utilized for cooling down a cavity mode, while the latter case of blue detuning may allow the self-excitation of oscillation. Operating close to the threshold of self-excited oscillation, i.e., close to the point where the total effective damping vanishes, may be useful for some sensing applications since the system is expected to become highly responsive to external perturbations near the threshold.

As was shown above, relatively large change in the damping rate can be induced provided that the Rabi frequency ω_{R} of the driven spins becomes comparable to the cavity mode frequency ω_{a} (see Fig. 5). Unfortunately, this region is inaccessible with the devices that have been investigated in the current experiment. However, in other CQED systems, the condition $\omega_{\mathrm{R}} \simeq \omega_{\mathrm{a}}$ can be more easily satisfied. For example, with superconducting CQED systems, both strong [20–23] and ultrastrong [24,25] coupling is possible. This, together with the ability to drive a Josephson qubit with Rabi frequencies high in the radio-frequency band, may allow satisfying the condition $\omega_{\mathrm{R}} \simeq \omega_{\mathrm{a}}$ with a strongly coupled cavity mode. As was shown above, a large change in cavity mode damping rate, of the order of $g_{\mathrm{a}}^2|p_0|/\gamma_2$, is possible provided that the region where $\omega_{\mathrm{R}} \simeq \omega_{\mathrm{a}}$ becomes accessible. For a typical superconducting CQED system, the damping rate of a decoupled cavity mode is far smaller than $g_{\mathrm{a}}^2|p_0|/\gamma_2$, and thus reaching this region may allow efficiently cooling down cavity modes by off-resonance qubit driving.

ACKNOWLEDGMENTS

We thank Denis Dikarov and Anton Sorkin for their help in microwave simulations of devices. This work was supported by the Israel Science Foundation, the Binational Science Foundation, the Security Research Foundation in the Technion, and the Russell Berrie Nanotechnology Institute. H.W. acknowledges financial support by the Shatz fellowships and by the Viterbi fellowships.

APPENDIX A: COUPLING TO DRIVEN SPINS

Consider an ensemble of spin-1/2 particles coupled to a cavity mode. The ensemble is characterized by a longitudinal (spin-lattice) relaxation rate γ_1 and by a transverse (spin-spin) relaxation rate γ_2. An external magnetic field is applied, having a component alternating with angular frequency ω_{p}, and an orthogonal static component. The amplitude of the alternating (static) component is $\gamma_{\mathrm{g}}^{-1}\omega_1$ ($\gamma_{\mathrm{g}}^{-1}\omega_{\mathrm{L}}$), where $\gamma_{\mathrm{g}} = 2\pi \times 28.03\,\mathrm{GHz\,T^{-1}}$ is the electron spin gyromagnetic ratio. It is assumed that driving is applied close to the electron spin resonance, i.e., $|\Delta_{\mathrm{pL}}| \ll \omega_{\mathrm{L}}$, where $\Delta_{\mathrm{pL}} = \omega_{\mathrm{p}} - \omega_{\mathrm{L}}$ is the detuning. The cavity mode is characterized by an angular frequency ω_{a} and a damping rate γ_{a}. The coupling between the cavity mode and the spin ensemble is characterized by a longitudinal coupling coefficient g_{a}.

1. Equations of motion

The Hamiltonian of the closed system is taken to be given by

$$\hbar^{-1}\mathcal{H}_{\mathrm{aL}} = \omega_{\mathrm{a}}\left(A_{\mathrm{a}}^{\dagger}A_{\mathrm{a}} + \frac{1}{2}\right) + \frac{\omega_{\mathrm{L}}}{2}\Sigma_z + \omega_1(e^{-i\omega_{\mathrm{p}}t}\Sigma_+ + e^{i\omega_{\mathrm{p}}t}\Sigma_-) - g_{\mathrm{a}}(A_{\mathrm{a}} + A_{\mathrm{a}}^{\dagger})\Sigma_z, \tag{A1}$$

where ω_{a} is the cavity mode angular frequency, A_{a} is a cavity annihilation operator, and Σ_z and $\Sigma_{\pm}$ are spin operators. The Heisenberg equations of motion are generated according to

$$\frac{dO}{dt} = -i[O,\hbar^{-1}\mathcal{H}_{\mathrm{aL}}], \tag{A2}$$

where O is an operator. Using the commutation relations

$$[A_{\mathrm{a}},A_{\mathrm{a}}^{\dagger}] = 1, \tag{A3}$$

$$[\Sigma_z,\Sigma_+] = 2\Sigma_+, \tag{A4}$$

$$[\Sigma_z,\Sigma_-] = -2\Sigma_-, \tag{A5}$$

$$[\Sigma_+,\Sigma_-] = \Sigma_z, \tag{A6}$$

one obtains

$$\frac{dA_{\mathrm{a}}}{dt} + i\omega_{\mathrm{a}}A_{\mathrm{a}} - ig_{\mathrm{a}}\Sigma_z = 0, \tag{A7}$$

$$\frac{d\Sigma_+}{dt} - i\Omega_{\mathrm{L}}\Sigma_+ + i\omega_1 e^{i\omega_{\mathrm{p}}t}\Sigma_z = 0, \tag{A8}$$

and

$$\frac{d\Sigma_z}{dt} + 2i\omega_1(\Sigma_+e^{-i\omega_{\mathrm{p}}t} - \Sigma_-e^{i\omega_{\mathrm{p}}t}) = 0, \tag{A9}$$

where

$$\Omega_{\mathrm{L}} = \omega_{\mathrm{L}} - 2g_{\mathrm{a}}(A_{\mathrm{a}} + A_{\mathrm{a}}^{\dagger}). \tag{A10}$$

In the next step, damping is introduced and the resultant equations for the operators A_{a}, Σ_+, and Σ_z are thermally averaged. This procedure leads to

$$\frac{da}{dt} + \Theta_{\mathrm{a}} = 0, \tag{A11}$$

$$\frac{dp_+}{dt} + \Theta_+ = 0, \tag{A12}$$

$$\frac{dp_z}{dt} + \Theta_z = 0, \tag{A13}$$

where

$$a = \langle A_{\mathrm{a}} \rangle, \tag{A14}$$

$$p_+ = e^{-i\omega_{\mathrm{p}}t}\langle \Sigma_+ \rangle, \tag{A15}$$

$$p_z = \langle \Sigma_z \rangle = p_z, \tag{A16}$$

triangle brackets denote thermal averaging, the functions Θ_{a}, Θ_+, and Θ_z are given by

$$\Theta_{\mathrm{a}} = \lambda_{\mathrm{a}} a - i g_{\mathrm{a}} p_z, \tag{A17}$$

$$\Theta_+ = (i\Delta_{\mathrm{pL}} + \gamma_2)p_+ + i\omega_1 p_z + 2ig_{\mathrm{a}}(a + a^*)p_+, \tag{A18}$$

$$\Theta_z = \gamma_1(p_z - p_0) + 2i\omega_1(p_+ - p_+^*), \tag{A19}$$

the cavity eigenvalue λ_{a} is given by $\lambda_{\mathrm{a}} = i\omega_{\mathrm{a}} + \gamma_{\mathrm{a}}$, the coefficient

$$p_0 = -\tanh\left(\frac{\hbar\omega_{\mathrm{L}}}{2k_{\mathrm{B}}T}\right) \tag{A20}$$

is the value of p_z in thermal equilibrium in the absence of both driving and coupling, k_{B} is the Boltzmann's constant. and T is the temperature.

2. The cavity eigenvalue

The 5×5 Jacobian matrix

$$J = \frac{\partial(\Theta_{\mathrm{a}},\Theta_{\mathrm{a}}^*,\Theta_+,\Theta_+^*,\Theta_z)}{\partial(a,a^*,p_+,p_+^*,p_z)} \tag{A21}$$

can be expressed as $J = J_0 + g_{\mathrm{a}}V$, where the matrix J_0 in a block form is given by

$$J_0 = \left(\begin{array}{cc|c} \lambda_{\mathrm{a}} & 0 & \\ 0 & \lambda_{\mathrm{a}}^* & 0 \\ \hline \multicolumn{2}{c|}{0} & J_{\mathrm{L}} \end{array}\right) \tag{A22}$$

the block J_{L} is given by

$$J_{\mathrm{L}} = \begin{pmatrix} i\Delta_{\mathrm{pL}} + \gamma_2 & 0 & i\omega_1 \\ 0 & -i\Delta_{\mathrm{pL}} + \gamma_2 & -i\omega_1 \\ 2i\omega_1 & -2i\omega_1 & \gamma_1 \end{pmatrix}, \tag{A23}$$

the matrix V is given by

$$V = \begin{pmatrix} 0 & 0 & 0 & 0 & -i \\ 0 & 0 & 0 & 0 & i \\ 2ip_+ & 2ip_+ & ix_{\mathrm{a}} & 0 & 0 \\ -2ip_+^* & -2ip_+^* & 0 & -ix_{\mathrm{a}} & 0 \\ 0 & 0 & 0 & 0 & 0 \end{pmatrix}, \tag{A24}$$

and

$$x_{\mathrm{a}} = 2(a + a^*). \tag{A25}$$

Let $\lambda_1,\lambda_2,\ldots,\lambda_5$ be the five eigenvalues of $J = J_0 + g_{\mathrm{a}}V$. In the limit $g_{\mathrm{a}} \to 0$, i.e., when the cavity mode is decoupled from the spins, it is assumed that $\lambda_1 \to \lambda_{\mathrm{a}}$. When g_{a} is sufficiently small, the eigenvalue λ_1, which henceforth is referred to as the cavity eigenvalue, can be calculated using perturbation theory. For the case of high-quality factor (i.e., the case where $\gamma_{\mathrm{a}} \ll \omega_{\mathrm{a}}$), λ_1 is found to be given to second order in g_{a} by

$$\lambda_1 = i\omega_{\mathrm{a}} + \gamma_{\mathrm{a}} + g_{\mathrm{a}}V_{11} - g_{\mathrm{a}}^2[VR(\omega_{\mathrm{a}})V]_{11} + O\left(g_{\mathrm{a}}^3\right), \tag{A26}$$

where the 5×5 matrix $R(\omega)$ in a block form is given by

$$R(\omega') = \left(\begin{array}{cc|c} 0 & 0 & \\ 0 & 0 & 0 \\ \hline \multicolumn{2}{c|}{0} & \chi_{\mathrm{L}}(\omega') \end{array}\right), \tag{A27}$$

where the 3×3 spin susceptibility matrix $\chi_{\mathrm{L}}(\omega')$ is given by

$$\chi_{\mathrm{L}}(\omega') = (J_{\mathrm{L}} - i\omega')^{-1}. \tag{A28}$$

With the help of Eq. (A24), one finds that

$$\lambda_1 = i\omega_{\mathrm{a}} + \gamma_{\mathrm{a}} + \Lambda_1 + O\left(g_{\mathrm{a}}^3\right), \tag{A29}$$

where

$$\Lambda_1 = 2g_{\mathrm{a}}^2\{p_+^*[\chi_{\mathrm{L}}(\omega_{\mathrm{a}})]_{32} - p_+[\chi_{\mathrm{L}}(\omega_{\mathrm{a}})]_{31}\}. \tag{A30}$$

The following holds [see Eq. (A23)]:

$$\chi_{\mathrm{L}}(\omega_{\mathrm{a}}) = \frac{1}{D_{\mathrm{L}}}\begin{pmatrix} D_2D_3 + 2\omega_1^2 & 2\omega_1^2 & -i\omega_1 D_2 \\ 2\omega_1^2 & D_1D_3 + 2\omega_1^2 & i\omega_1 D_1 \\ -2i\omega_1 D_2 & 2i\omega_1 D_1 & D_1D_2 \end{pmatrix}, \tag{A31}$$

where

$$D_1 = i\Delta_{\mathrm{pL}} + \gamma_2 - i\omega_{\mathrm{a}}, \tag{A32}$$

$$D_2 = -i\Delta_{\mathrm{pL}} + \gamma_2 - i\omega_{\mathrm{a}}, \tag{A33}$$

$$D_3 = \gamma_1 - i\omega_{\mathrm{a}}, \tag{A34}$$

$$D_{\mathrm{L}} = D_1D_2D_3 + 2\omega_1^2(D_1 + D_2). \tag{A35}$$

The determinant D_{L} can be expressed as [see Eq. (A35)]

$$\frac{D_{\mathrm{L}}}{\omega_{\mathrm{a}}^3} = \frac{\gamma_1}{\omega_{\mathrm{a}}}\left(\frac{\Delta_{\mathrm{pL}}^2 - \omega_{\mathrm{dR}}^2}{\omega_{\mathrm{a}}^2}\right) - i\left(\frac{\Delta_{\mathrm{pL}}^2 - \omega_{\mathrm{dI}}^2}{\omega_{\mathrm{a}}^2}\right), \tag{A36}$$

where

$$\frac{\omega_{\mathrm{dR}}}{\omega_{\mathrm{a}}} = \sqrt{1 + \frac{2\gamma_2}{\gamma_1}\left(1 - \frac{2\omega_1^2}{\omega_{\mathrm{a}}^2}\right) - \frac{\gamma_2^2}{\omega_{\mathrm{a}}^2}} \tag{A37}$$

and

$$\frac{\omega_{\mathrm{dI}}}{\omega_{\mathrm{a}}}=\sqrt{1-\frac{4\omega_1^2}{\omega_{\mathrm{a}}^2}-\frac{(2\gamma_1+\gamma_2)\gamma_2}{\omega_{\mathrm{a}}^2}}. \tag{A38}$$

Using these notations, Eq. (A30) becomes

$$\frac{\Lambda_1}{\omega_{\mathrm{a}}}=\frac{8g_{\mathrm{a}}^2\omega_1}{\omega_{\mathrm{a}}^3}\frac{ip_+''\frac{\Delta_{\mathrm{pL}}}{\omega_{\mathrm{a}}}+p_+'\left(1+i\frac{\gamma_2}{\omega_{\mathrm{a}}}\right)}{\frac{D_{\mathrm{L}}}{\omega_{\mathrm{a}}^3}}, \tag{A39}$$

where p_+' (p_+'') is the real (imaginary) part of p_+, i.e.,

$$p_+'=\frac{p_++p_+^*}{2}, \tag{A40}$$

$$p_+''=\frac{p_+-p_+^*}{2i}. \tag{A41}$$

To second order in g_{a}, the term Λ_1 [see Eq. (A39)] can be calculated by evaluating the fixed point value of p_+ to zeroth order in g_{a}, which is done by solving the set of equations $\Theta_{\mathrm{a}}=0$, $\Theta_+=0$, and $\Theta_z=0$ for the case $g_{\mathrm{a}}=0$. The steady-state values of the variables a, p_+, and p_z are found to be given by $a_0=0$,

$$p_{+0}=\frac{\frac{\omega_1}{\gamma_2}\left(-\frac{\Delta_{\mathrm{pL}}}{\gamma_2}-i\right)p_0}{1+\frac{\Delta_{\mathrm{pL}}^2}{\gamma_2^2}+\frac{4\omega_1^2}{\gamma_1\gamma_2}}, \tag{A42}$$

$$p_{z0}=\frac{\left(1+\frac{\Delta_{\mathrm{pL}}^2}{\gamma_2^2}\right)p_0}{1+\frac{\Delta_{\mathrm{pL}}^2}{\gamma_2^2}+\frac{4\omega_1^2}{\gamma_1\gamma_2}}, \tag{A43}$$

respectively. For the case where $\gamma_1,\gamma_2\ll\omega_{\mathrm{a}}$, Eqs. (A37) and (A38) become

$$\frac{\omega_{\mathrm{dR}}}{\omega_{\mathrm{a}}}=\sqrt{1+\frac{2\gamma_2}{\gamma_1}\left(1-\frac{2\omega_1^2}{\omega_{\mathrm{a}}^2}\right)} \tag{A44}$$

and

$$\frac{\omega_{\mathrm{dI}}}{\omega_{\mathrm{a}}}=\sqrt{1-\frac{4\omega_1^2}{\omega_{\mathrm{a}}^2}}. \tag{A45}$$

With the help of Eqs. (A36), (A39), (A44), and (A45), one obtains, for this case,

$$\frac{\Lambda_1}{\omega_{\mathrm{a}}}=-\frac{\frac{\frac{8g_{\mathrm{a}}^2\omega_1^2}{\omega_{\mathrm{a}}^3\gamma_2}\frac{\Delta_{\mathrm{pL}}}{\gamma_2}\left(1+\frac{2i\gamma_2}{\omega_{\mathrm{a}}}\right)}{1+\frac{\Delta_{\mathrm{pL}}^2}{\gamma_2^2}+\frac{4\omega_1^2}{\gamma_1\gamma_2}}p_0}{\frac{\gamma_1}{\omega_{\mathrm{a}}}\left(\frac{\omega_{\mathrm{R}}^2+\eta\omega_{\mathrm{a}}^2}{\omega_{\mathrm{a}}^2}-1\right)-i\left(\frac{\omega_{\mathrm{R}}^2}{\omega_{\mathrm{a}}^2}-1\right)}, \tag{A46}$$

where

$$\eta=\frac{2\gamma_2}{\gamma_1}\left[\left(1-\frac{\gamma_1}{\gamma_2}\right)\frac{2\omega_1^2}{\omega_{\mathrm{a}}^2}-1\right], \tag{A47}$$

and where $\omega_{\mathrm{R}}=\sqrt{4\omega_1^2+\Delta_{\mathrm{pL}}^2}$ is the Rabi frequency of the driven spins.

APPENDIX B: INTERMODE COUPLING

In general, Eq. (A26) can be employed for calculating the eigenvalue of a cavity mode that is weakly coupled to any given ancilla system. In the previous section, the ancilla system under consideration was an ensemble of driven spins, whereas in the current section the ancilla system is taken to be the driven spiral mode. In general, the second-order term $-g^2[VR(\omega_{\mathrm{a}})V]_{11}$ in Eq. (A26) can be calculated by evaluating the steady-state response of the ancilla system to small monochromatic oscillations of the cavity mode at its own resonance frequency. Substituting the steady-state solution into the equation of motion of the cavity mode gives its eigenvalue. This approach will be employed in this section.

The Hamiltonian of the two-mode cavity closed system is taken to be given by

$$\hbar^{-1}\mathcal{H}_{\mathrm{ab}}=\omega_{\mathrm{a}}\left(A_{\mathrm{a}}^\dagger A_{\mathrm{a}}+\tfrac{1}{2}\right)+\omega_{\mathrm{b}}\left(A_{\mathrm{b}}^\dagger A_{\mathrm{b}}+\tfrac{1}{2}\right)+K(A_{\mathrm{a}}+A_{\mathrm{a}}^\dagger)(A_{\mathrm{b}}+A_{\mathrm{b}}^\dagger)^2, \tag{B1}$$

where ω_{a} and A_{a} (ω_{b} and A_{b}) are the angular frequency and the annihilation operator, respectively, of the omega (spiral) resonator, and K is the intermode coupling coefficient. The Heisenberg equations of motion are given by [see Eq. (A2)]

$$\frac{dA_{\mathrm{a}}}{dt}+i\omega_{\mathrm{a}}A_{\mathrm{a}}+iK(A_{\mathrm{b}}+A_{\mathrm{b}}^\dagger)^2=0, \tag{B2}$$

$$\frac{dA_{\mathrm{b}}}{dt}+i\omega_{\mathrm{b}}A_{\mathrm{b}}+2iK(A_{\mathrm{a}}+A_{\mathrm{a}}^\dagger)(A_{\mathrm{b}}+A_{\mathrm{b}}^\dagger)=0. \tag{B3}$$

Adding damping and driving leads to

$$\frac{dA_{\mathrm{a}}}{dt}+(i\omega_{\mathrm{a}}+\gamma_{\mathrm{a}})A_{\mathrm{a}}+iK(A_{\mathrm{b}}+A_{\mathrm{b}}^\dagger)^2=F_{\mathrm{a}} \tag{B4}$$

and

$$\frac{dA_{\mathrm{b}}}{dt}+(i\omega_{\mathrm{b}}+\gamma_{\mathrm{b}})A_{\mathrm{b}}+2iK(A_{\mathrm{a}}+A_{\mathrm{a}}^\dagger)(A_{\mathrm{b}}+A_{\mathrm{b}}^\dagger)=F_{\mathrm{bf}}e^{-i(\omega_{\mathrm{b}}+\omega_{\mathrm{D}})t}+F_{\mathrm{b}}, \tag{B5}$$

where both noise terms F_{a} and F_{b} have a vanishing expectation value. Averaging yields

$$\frac{d\mathcal{A}_{\mathrm{a}}}{dt}+(i\omega_{\mathrm{a}}+\gamma_{\mathrm{a}})\mathcal{A}_{\mathrm{a}}+iK(\mathcal{A}_{\mathrm{b}}+\mathcal{A}_{\mathrm{b}}^*)^2=0 \tag{B6}$$

and

$$\frac{d\mathcal{A}_{\mathrm{b}}}{dt}+(i\omega_{\mathrm{b}}+\gamma_{\mathrm{b}})\mathcal{A}_{\mathrm{b}}+S_{\mathrm{b}1}+S_{\mathrm{b}2}=F_{\mathrm{bf}}e^{-i(\omega_{\mathrm{b}}+\omega_{\mathrm{D}})t}, \tag{B7}$$

where

$$\langle A_{\mathrm{a}}\rangle=\mathcal{A}_{\mathrm{a}}=a_{\mathrm{a}}e^{-i\omega_{\mathrm{a}}t}, \tag{B8}$$

$$\langle A_{\mathrm{b}}\rangle=\mathcal{A}_{\mathrm{b}}=a_{\mathrm{b}}e^{-i\omega_{\mathrm{b}}t}, \tag{B9}$$

and where

$$S_{\mathrm{b}1}=2iK(\mathcal{A}_{\mathrm{a}}+\mathcal{A}_{\mathrm{a}}^*)\mathcal{A}_{\mathrm{b}}, \tag{B10}$$

$$S_{\mathrm{b}2}=2iK(\mathcal{A}_{\mathrm{a}}+\mathcal{A}_{\mathrm{a}}^*)\mathcal{A}_{\mathrm{b}}^*. \tag{B11}$$

In the sections below, the effect of the terms $S_{\mathrm{b}1}$ and $S_{\mathrm{b}2}$ is separately evaluated.

1. The effect of the S_{b1} term

When the term S_{b2} is disregarded, Eq. (B7) becomes

$$\frac{dC_b}{dt} + (i\Omega_b + \gamma_b)C_b = F_{bf}, \tag{B12}$$

where

$$\Omega_b = -\omega_D + 2K(\mathcal{A}_a + \mathcal{A}_a^*), \tag{B13}$$

and where

$$\mathcal{A}_b = C_b e^{-i(\omega_b+\omega_D)t}. \tag{B14}$$

By employing the notation

$$C_b = C_{b0} + c_b, \tag{B15}$$

where

$$C_{b0} = \frac{F_{bf}}{-i\omega_D + \gamma_b}, \tag{B16}$$

one obtains, in the limit of small K,

$$\frac{dc_b}{dt} + (-i\omega_D + \gamma_b)c_b = -2iK(\mathcal{A}_a + \mathcal{A}_a^*)C_{b0}. \tag{B17}$$

Let $\mathcal{A}_a = a_a e^{-i\omega_a t}$ [see Eq. (B8)] and assume that a_a is constant. The steady-state solution reads

$$c_b = \frac{2iKC_{b0}\mathcal{A}_a}{i(\omega_D + \omega_a) - \gamma_b} + \frac{2iKC_{b0}\mathcal{A}_a^*}{i(\omega_D - \omega_a) - \gamma_b}. \tag{B18}$$

When only terms proportional to $\mathcal{A}_a$ are kept, one finds the coupling term in Eq. (B6) can be expressed as

$$iK(\mathcal{A}_b + \mathcal{A}_b^*)^2 \simeq \frac{4iK^2|C_{b0}|^2\omega_D\mathcal{A}_a}{[i(\omega_a - \omega_D) - \gamma_b][i(\omega_a + \omega_D) - \gamma_b]}. \tag{B19}$$

2. The effect of the S_{b2} term

For this case, the term S_{b1} in Eq. (B7) is disregarded. Furthermore, the counter-rotating term proportional to $\mathcal{A}_a^*\mathcal{A}_b^*$ is disregarded as well [see Eq. (B11)]. For this case, Eq. (B7) becomes

$$\frac{da_b}{dt} + \gamma_b a_b + 2iKa_a a_b^* e^{i\omega_s t} = F_{bf}e^{-i\omega_D t}, \tag{B20}$$

where

$$\omega_s = 2\omega_b - \omega_a. \tag{B21}$$

Consider a solution of Eq. (B20) having the form [26]

$$a_b = \alpha e^{-i\omega_D t} + \beta e^{i(\omega_s+\omega_D)t}. \tag{B22}$$

Substituting the solution into Eq. (B20) and assuming that α, β, and a_a are all constants lead to

$$(-i\omega_D + \gamma_b)\alpha + 2iKa_a\beta^* = F_{bf} \tag{B23}$$

and

$$[i(\omega_s + \omega_D) + \gamma_b]\beta + 2iKa_a\alpha^* = 0, \tag{B24}$$

thus

$$\alpha = \frac{F_{bf}}{-i\omega_D + \gamma_b - \frac{4K^2|a_a|^2}{-i(\omega_s+\omega_D)+\gamma_b}} \tag{B25}$$

and

$$\beta = \frac{-2iKa_a\alpha^*}{i(\omega_s + \omega_D) + \gamma_b}. \tag{B26}$$

The steady-state solution (B22) can be used to express the coupling term $iK(\mathcal{A}_b + \mathcal{A}_b^*)^2$ in Eq. (B6) in terms of $\mathcal{A}_a$. To that end, $\mathcal{A}_b$ is expressed as [see Eqs. (B8), (B22), and (B26)]

$$\begin{aligned}\mathcal{A}_b &= \alpha e^{-i(\omega_b+\omega_D)t} + \beta e^{i(\omega_b+\omega_D-\omega_a)t} \\ &= \alpha e^{-i(\omega_b+\omega_D)t} - \frac{2iK\alpha^* e^{i(\omega_b+\omega_D)t}}{i(\omega_s + \omega_D) + \gamma_b}\mathcal{A}_a.\end{aligned} \tag{B27}$$

When only terms proportional to $\mathcal{A}_a$ are kept, the following approximation is employed [see Eq. (B25)]:

$$\alpha \simeq \frac{F_{bf}}{-i\omega_D + \gamma_b}, \tag{B28}$$

and it is assumed that $|\omega_D| \ll |\omega_s|$ for evaluating β [see Eq. (B26)], the coupling term in Eq. (B6) becomes

$$\begin{aligned}iK(\mathcal{A}_b + \mathcal{A}_b^*)^2 &\simeq -\frac{4K^2|\alpha|^2\mathcal{A}_a}{i(\omega_s + \omega_D) + \gamma_b} \\ &\simeq -\frac{4K^2|F_{bf}|^2\mathcal{A}_a}{(i\omega_s + \gamma_b)(\omega_D^2 + \gamma_b^2)}.\end{aligned} \tag{B29}$$

When $\gamma_b \ll \omega_s$, one has

$$iK(\mathcal{A}_b + \mathcal{A}_b^*)^2 \simeq \frac{4K^2|F_{bf}|^2(i\omega_s - \gamma_b)\mathcal{A}_a}{\omega_s^2(\omega_D^2 + \gamma_b^2)}. \tag{B30}$$

[1] S. Haroche and D. Kleppner, Cavity quantum electrodynamics, Phys. Today **42**, 24 (1989).

[2] B. W. Shore and P. L. Knight, The Jaynes-Cummings model, J. Mod. Opt. **40**, 1195 (1993).

[3] E. Buks, C. Deng, J.-L. F. X. Orgazzi, M. Otto, and A. Lupascu, Superharmonic resonances in a strongly coupled cavity-atom system, Phys. Rev. A **94**, 033807 (2016).

[4] S. Ates, S. M. Ulrich, A. Ulhaq, S. Reitzenstein, A. Löffler, S. Höfling, A. Forchel, and P. Michler, Nonresonant dot-cavity coupling and its potential for resonant single-quantum-dot spectroscopy, Nat. Photon. **3**, 724 (2009).

[5] A. Ghirri, C. Bonizzoni, F. Troiani, N. Buccheri, L. Beverina, A. Cassinese, and M. Affronte, Coherently coupling distinct spin ensembles through a high-T_c superconducting resonator, Phys. Rev. A **93**, 063855 (2016).

[6] Y. S. Yap, H. Yamamoto, Y. Tabuchi, M. Negoro, A. Kagawa, and M. Kitagawa, Strongly driven electron spins using a k_u band stripline electron paramagnetic resonance resonator, J. Magn. Reson. **232**, 62 (2013).

[7] A. Ghirri, C. Bonizzoni, D. Gerace, S. Sanna, A. Cassinese, and M. Affronte, $YBa_2Cu_3O_7$ microwave resonators for strong

collective coupling with spin ensembles, Appl. Phys. Lett. **106**, 184101 (2015).

[8] T. Ramos, V. Sudhir, K. Stannigel, P. Zoller, and T. J. Kippenberg, Nonlinear Quantum Optomechanics via Individual Intrinsic Two-Level Defects, Phys. Rev. Lett. **110**, 193602 (2013).

[9] L. Ella and E. Buks, Hopf bifurcation in a flux qubit coupled to a nanomechanical oscillator, arXiv:1210.6902.

[10] M. Grajcar, S. H. W. V. D. Ploeg, A. Izmalkov, E. Ilichev, H.-G. Meyer, A. Fedorov, A. Shnirman, and G. Schön, Sisyphus cooling and amplification by a superconducting qubit, Nat. Phys. **4**, 612 (2008).

[11] J. M. de Voogd, J. J. T. Wagenaar, and T. H. Oosterkamp, Dissipation and resonance frequency shift of a resonator magnetically coupled to a semiclassical spin, Sci. Rep. **7**, 42239 (2017).

[12] R. Glenn and M. E. Raikh, Rabi-vibronic resonance with large number of vibrational quanta, Phys. Rev. B **84**, 195454 (2011).

[13] Y. Twig, E. Suhovoy, and A. Blank, Sensitive surface loop-gap microresonators for electron spin resonance, Rev. Sci. Instrum. **81**, 104703 (2010).

[14] N. Maleeva, M. Fistul, A. Averkin, A. Karpov, and A. V. Ustinov, Electrodynamics of a spiral resonator as a suitable magnetic component of metamaterials, Proc. Metamater. 474 (2013).

[15] N. Maleeva, M. V. Fistul, A. Karpov, A. P. Zhuravel, A. Averkin, P. Jung, and A. V. Ustinov, Electrodynamics of a ring-shaped spiral resonator, J. Appl. Phys. **115**, 064910 (2014).

[16] D. E. Kaplan, M. E. Browne, and J. A. Cowen, Pulsed x-band EPR spectrometer, Rev. Sci. Instrum. **32**, 1182 (1961).

[17] J. P. Lloyd and G. E. Pake, Spin-lattice relaxation and the residual width of highly exchange-narrowed paramagnetic resonances, Phys. Rev. **92**, 1576 (1953).

[18] D. I. Schuster, A. P. Sears, E. Ginossar, L. DiCarlo, L. Frunzio, J. J. L. Morton, H. Wu, G. A. D. Briggs, B. B. Buckley, D. D. Awschalom, and R. J. Schoelkopf, High-Cooperativity Coupling of Electron-Spin Ensembles to Superconducting Cavities, Phys. Rev. Lett. **105**, 140501 (2010).

[19] M. Aspelmeyer, T. J. Kippenberg, and F. Marquardt, Cavity optomechanics, Rev. Mod. Phys. **86**, 1391 (2014).

[20] A. A. Houck, J. A. Schreier, B. R. Johnson, J. M. Chow, J. Koch, J. M. Gambetta, D. I. Schuster, L. Frunzio, M. H. Devoret, S. M. Girvin, and R. J. Schoelkopf, Controlling the Spontaneous Emission of a Superconducting Transmon Qubit, Phys. Rev. Lett. **101**, 080502 (2008).

[21] A. Blais, R.-S. Huang, A. Wallraff, S. M. Girvin, and R. J. Schoelkopf, Cavity quantum electrodynamics for superconducting electrical circuits: An architecture for quantum computation, Phys. Rev. A **69**, 062320 (2004).

[22] J. Koch, M. Y. Terri, J. Gambetta, A. A. Houck, D. I. Schuster, J. Majer, A. Blais, M. H. Devoret, S. M. Girvin, and R. J. Schoelkopf, Charge-insensitive qubit design derived from the Cooper pair box, Phys. Rev. A **76**, 042319 (2007).

[23] A. Wallraff, D. I. Schuster, A. Blais, L. Frunzio, R.-S. Huang, J. Majer, S. Kumar, S. M. Girvin, and R. J. Schoelkopf, Strong coupling of a single photon to a superconducting qubit using circuit quantum electrodynamics, Nature (London) **431**, 162 (2004).

[24] T. Niemczyk, F. Deppe, H. Huebl, E. P. Menzel, F. Hocke, M. J. Schwarz, J. J. Garcia-Ripoll, D. Zueco, T. Hümmer, E. Solano, A. Marx, and R. Gross, Circuit quantum electrodynamics in the ultrastrong-coupling regime, Nat. Phys. **6**, 772 (2010).

[25] P. F.-Díaz, J. Lisenfeld, D. Marcos, J. J. García-Ripoll, E. Solano, C. J. P. M. Harmans, and J. E. Mooij, Observation of the Bloch-Siegert Shift in a Qubit-Oscillator System in the Ultrastrong Coupling Regime, Phys. Rev. Lett. **105**, 237001 (2010).

[26] R. Lifshitz and M. C. Cross, Nonlinear dynamics of nanomechanical and micromechanical resonators, in *Reviews of Nonlinear Dynamics and Complexity*, edited by Heinz Georg Schuster (Wiley-VCH, New York, 2008), Vol. 1, pp. 1–48.